parameters of the conventional sequence for the single slice scan were: TR/TE/θ = 60 ms/40 ms/20°; slice thickness, 5 mm; in-plane resolution, 1.0 mm × 1.0 mm. In the conventional gradient-echo fMRI experiment, 135 images were acquired when the subject performed three cycles of rest, control and TOD. Each block lasted 180 s and comprised 15 conventional fMRI images. We acquired anatomical images to localize the subcortical nuclei, which had clear boundaries on the T_2^*-weighted images.

Data analysis. We used a MEDX software package (Sensor Systems) and in-house programs for image processing, including corrections for head motion and global MRI signal shift. For each voxel, we denote I_0 as the mean MRI signal intensity at the resting condition, which was the average of all images acquired during the three blocks of Rest. The relative MRI signal intensity, $S_{block}(n)$, during each block was defined as[17,24] $S_{block}(n) = [I_{block}(n) - I_0]/I_0$ $(n = 1, 2 \ldots N)$ where $I_{block}(n)$ is the MRI signal intensity of the nth image in a block (rest, control or TOD), and N is the number of total images acquired in each block. The TOD-induced activation was then determined by comparing the mean of $S_{TOD}(n)$ and the mean of $S_{Control}(n)$, using group t-tests and a pixel-clustering technique[28]. The resulting t-maps and their corresponding T_2^* images were then co-registered with the anatomical images using spatial normalization[29].

Analyses of the inter-regional covariance were performed on $S_{Rest}(n)$, and $\Delta S(n) = S_{TOD}(n) - S_{Rest}(n)$. At each image in the time series, we calculated $\Delta S(n)$ by paired subtraction between blocks (that is, the first image in TOD minus the first image in Rest, and so on). The time course in an active ROI (defined on the t-maps, see above) was then measured by averaging $\Delta S(n)$ on the number of pixels in the ROI. The resulting spatially averaged time courses of $\Delta S(n)$ in the ROIs (dentate nucleus, globus pallidus, SMA, M1 and PFC) are shown in Fig. 1. The covariance maps were generated on a pixel-by-pixel basis by correlating the time course in a reference ROI (for example, an active region in the dentate nucleus) with those in the pixels throughout the image(s). The cross correlation (r) was calculated using the method from a previous study of fMRI time courses[18]. Here we only utilized the time series within the period of a block, and used the time series averaged on an active region as the reference function, a method that is independent of the blocked paradigm. The significance of r (versus zero) was determined by one-tail paired t tests ($N = 20$ or 15). The same spatial normalization procedure and clustering size were used for generating the covariance maps.

Received 5 March; accepted 1 June 1999.

1. Allen, G. I. & Tsukahara, N. Cerebrocerebellar communication systems. *Physiol. Rev.* **54,** 957–1006 (1974).
2. Marsden, C. D. The mysterious motor function of the basal ganglia: The Robert Wartenberg Lecture. *Neurology* **32,** 514–539 (1984).
3. Houk, J. C. & Wise, S. P. Distributed modular architecture linking basal ganglia, cerebellum, and cerebral cortex: their role in planning and controlling action. *Cereb. Cortex* **5,** 95–110 (1995).
4. Ghez, C. in *Principles of Neural Sciences* (eds Kandel, E. R., Schwarts, J. H. & Jessel, T. M.) 609–625 (Elsevier, New York, 1991).
5. Rouiller, E. M. in *Hand and Brain* (eds Wing, A. M., Haggard, P. & Flanagan, J. R.) 99–124 (Academic, San Diego, 1996).
6. Hoover, J. E. & Strick, P. L. Multiple output channels in the basal ganglia. *Science* **259,** 819–821 (1993).
7. Hoover, J. E. & Strick, P. L. The organization of cerebellar and basal ganglia outputs to primary motor cortex as revealed by retrograde transneuronal transport of herpes simplex virus type 1. *J. Neurosci.* **19,** 1446–1463 (1999).
8. Middleton, F. A. & Strick, P. L. Dentate output channels: motor and cognitive components. *Prog. Brain Res.* **114,** 553–566 (1997).
9. Middleton, F. A. & Strick, P. L. Anatomical evidence for cerebellar and basal ganglia involvement in higher cognitive function. *Science* **266,** 458–461 (1994).
10. Houk, J. C. On the role of the cerebellum and basal ganglia in cognitive signal processing. *Prog. Brain Res.* **114,** 543–552 (1997).
11. Voogd, J. & Ruigrok, T. J. H. Transverse and longitudinal patterns in the mammalian cerebellum. *Prog. Brain Res.* **114,** 21–37 (1997).
12. Graybiel, A. M., Aosaki, T., Flaherty, A. W. & Kimura, M. The basal ganglia and adaptive motor control. *Science* **265,** 1826–1831 (1994).
13. Churchland, P. S. & Sejnowski, T. J. Perspectives in cognitive neuroscience. *Science* **242,** 741–745 (1988).
14. Bressler, S. L. Large-scale cortical networks and cognition. *Brain Res. Rev.* **20,** 288–304 (1995).
15. Van Essen, D. C., Anderson, C. H. & Olshausen, B. A. in *Large-Scale Neuronal Theories of the Brain* (eds Kock, C. & Davis, J. L.) 271–299 (MIT Press, Cambridge, Massachusetts, 1994).
16. Kwong, K. K. *et al.* Dynamic magnetic resonance of human brain activity during primary sensory stimulation. *Proc. Natl Acad. Sci. USA* **89,** 5675–5679 (1992).
17. Ogawa, S. *et al.* Functional brain mapping by blood oxygenation level-dependent contrast magnetic resonance imaging. *J. Biophys.* **64,** 803–812 (1993).
18. Bandettini, P. A., Jesmanowicz, A., Wong, E. C. & Hyde, J. S. Processing strategies for time course data sets in functional MRI of the human brain. *Magn. Reson. Med.* **30,** 161–173 (1993).
19. Gao, J. H. *et al.* Cerebellum implicated in sensory acquisition and discrimination rather than motor control. *Science* **272,** 545–547 (1996).
20. Cohen, J. D. *et al.* Temporal dynamics of bran activation during a working memory task. *Nature* **386,** 604–608 (1997).
21. Courtney, S. M., Ungerleider, L. G., Keil, K. & Haxby, J. V. Transient and sustained activity in a distributed neural system for human working memory. *Nature* **386,** 608–611 (1997).
22. Houk, J. C., Keifer, J. & Barto, A. G. Distributed commands in the limb premotor network. *Trends Neurosci.* **16,** 27–33 (1993).
23. Liu, Y. *et al.* Involvement of the human red nucleus in sensory discrimination. *Proc. Int. Soc. Magn. Reson. Med.* **6,** 110 (1998).
24. Friston, K. J. *et al.* Analysis of fMRI time-series revised. *NeuroImage* **2,** 45–53 (1995).
25. Biswal, B., Yetkin, F. Z., Haughton, V. M. & Hyde, J. S. Functional connectivity in the motor cortex of resting human brain using echo-planar MRI. *Magn. Reson. Med.* **34,** 537–541 (1995).
26. Friston, K. J., Frith, C. D., Liddle, P. F. & Frackowiak, R. S. J. Functional connectivity: the principle-component analysis of large (PET) data sets. *J. Cereb. Blood Flow Metab.* **13,** 5–14 (1993).
27. Roland, P. E., Eriksson, L., Widen, L. & Stone-Elander, S. Changes in regional cerebral oxidative metabolism induced by tactile learning and recognition in man. *Eur. J. Neurosci.* **1,** 3–18 (1988).
28. Xiong, J., Gao, J. H., Lancaster, J. L. & Fox, P. T. Clustered pixels analysis for functional MRI activation studies of the human brain. *Hum. Brain Mapp.* **3,** 287–301 (1995).
29. Fox, P. T. Spatial normalization: origins, applications, and alternatives. *Hum. Brain Mapp.* **4,** 1–2 (1995).

Acknowledgements. We thank J. C. Houk for comments on the manuscript.

Correspondence and requests for materials should be addressed to Y.L. (e-mail: LIUY1@uthscsa.edu).

Sensory experience modifies the short-term dynamics of neocortical synapses

Gerald T. Finnerty*, Langdon S. E. Roberts & Barry W. Connors

Department of Neuroscience, Brown University, Providence, Rhode Island 02912, USA

Many representations of sensory stimuli in the neocortex are arranged as topographic maps. These cortical maps are not fixed, but show experience-dependent plasticity[1,2]. For instance, sensory deprivation causes the cortical area representing the deprived sensory input to shrink, and neighbouring spared representations to enlarge, in somatosensory[3], auditory[4] or visual cortex[5]. In adolescent and adult animals, changes in cortical maps are most noticeable in the supragranular layers at the junction of deprived and spared cortex[6–9]. However, the cellular mechanisms of this experience-dependent plasticity are unclear. Long-term potentiation and depression have been implicated[10–12], but have not been proven to be necessary or sufficient for cortical map reorganization. Short-term synaptic dynamics have not been considered. We developed a brain slice preparation involving rat whisker barrel cortex *in vitro*. Here we report that sensory deprivation alters short-term synaptic dynamics in both vertical and horizontal excitatory pathways within the supragranular cortex. Moreover, modifications of horizontal pathways amplify changes in the vertical inputs. Our findings help to explain the functional cortical reorganization that follows persistent changes of sensory experience.

Rats obtain detailed sensory information from their facial whiskers[13]. The five rows of whiskers and corresponding whisker barrel rows in the contralateral primary somatosensory cortex are conventionally labelled A to E[14] (Fig. 1a). We altered the sensory experience of rats by trimming bilaterally either the dorsal three rows (A–C) or the ventral two rows (D, E) of whiskers flush with the skin every day for 10 days beginning at P11–15. Thus, the junction between cortex which had lost its sensory input ('deprived') and that which had retained its input ('spared') was always between the C and D barrel rows. A third sham-trimmed group served as a control. We cut brain slices across the rat whisker barrel rows (Fig. 1a, b). Transilluminating slices allowed reliable visual identification of the barrel rows and, thus, of the junction between deprived and spared cortex. Layer 2/3 pyramidal neurons in the deprived, spared and control cortex did not differ in resting membrane potential, input resistance, membrane capacitance and spike threshold (Table 1), indicating that sensory deprivation did

* Present address: Department of Physiology, School of Medical Sciences, University Walk, Bristol BS8 1TD, UK.

not alter intrinsic cellular properties. We studied the short-term dynamics of excitatory synapses onto layer 2/3 pyramidal cells. Vertical or horizontal intracortical pathways were stimulated with three trains of eleven stimuli at 2–40 Hz with 30 s separation between trains (Fig. 1c, d). EPSP amplitudes were normalized with respect to the first response and the last three responses were averaged to estimate the normalized steady-state amplitude (Fig. 2a). EPSP amplitudes during a train depressed at all stimulation frequencies, as found in other cortical areas[15,16]. We fitted single exponential curves to find the time constant of EPSP amplitude decay (Fig. 2a). The amount of depression increased with stimulation frequency in both horizontal (Fig. 2b, f) and vertical pathways (Fig. 3b).

Sensory deprivation caused complex changes in synaptic dynamics. We compared horizontal inputs from spared and deprived cortex onto deprived layer 2/3 neurons. The amount of steady-state depression was greater in spared-to-deprived inputs compared with deprived-to-deprived inputs at all stimulation frequencies tested ($P = 0.01$, paired t-test, $n = 12$) (Fig. 2b, c). Depression of control cortex was intermediate between that recorded from deprived and spared cortex. We found that deprived-to-deprived inputs depressed significantly less than controls (mean difference, 0.07 ± 0.02, $P = 0.02$, paired t-test) whereas spared-to-deprived inputs tended to depress more. This indicated that horizontal inputs to deprived cortex were modified by sensory deprivation, but in opposite ways depending on their source. The increase in depression found in the spared-to-deprived input compared to the deprived-to-deprived input was accompanied by a shortening of the time constant of EPSP amplitude decay (mean decrease, $28 \pm 5\%$, $P = 0.03$, paired t-test) (Fig. 2d). A similar analysis of pathways to spared cortex showed that inputs from deprived and spared cortex depressed by comparable amounts and at similar rates (Fig. 2e). The depression of spared inputs was greater than control (mean difference, 0.06 ± 0.02, $P = 0.04$, paired t-test), and deprived inputs were similar to spared inputs (Fig. 2f).

Table 1 Intrinsic properties of layer 2/3 pyramidal cells

	Control	Deprived	Spared
Resting membrane potential (mV)	-79 ± 2	-78 ± 2	-76 ± 1
Input resistance (MΩ)	61 ± 4	53 ± 3	48 ± 5
Membrane capacitance (pF)	260 ± 20	290 ± 20	260 ± 20
Threshold – resting membrane potential (mV)	26 ± 1	25 ± 2	26 ± 2

All data are shown as mean ± s.e.m. One-way analysis of variance showed no difference in resting membrane potential ($n = 32$, $F_{2,29} = 1.21$, $P = 0.313$), input resistance ($n = 35$, $F_{2,32} = 2.218$, $P = 0.125$), membrane capacitance ($n = 35$, $F_{2,32} = 0.894$, $P = 0.419$) or threshold minus resting membrane potential ($n = 15$, $F_{2,12} = 0.138$, $P = 0.872$).

Sensory deprivation also influenced the dynamics of vertical pathways onto layer 2/3 pyramidal cells. The relationship between normalized steady-state amplitude and frequency was significantly different when comparing the vertical layer 4–2 pathways in deprived and spared cortex ($P < 0.01$, paired t-test, $n = 13$). More detailed analysis revealed that, unlike horizontal inputs to deprived cortex, responses were not modified equally at all stimulation frequencies. Spared cortex depressed significantly more than the deprived cortex at 5 and 10 Hz ($P = 0.043$ and 0.047, respectively, paired t-tests, $n = 13$) (Fig. 3a), but less difference was seen at 20

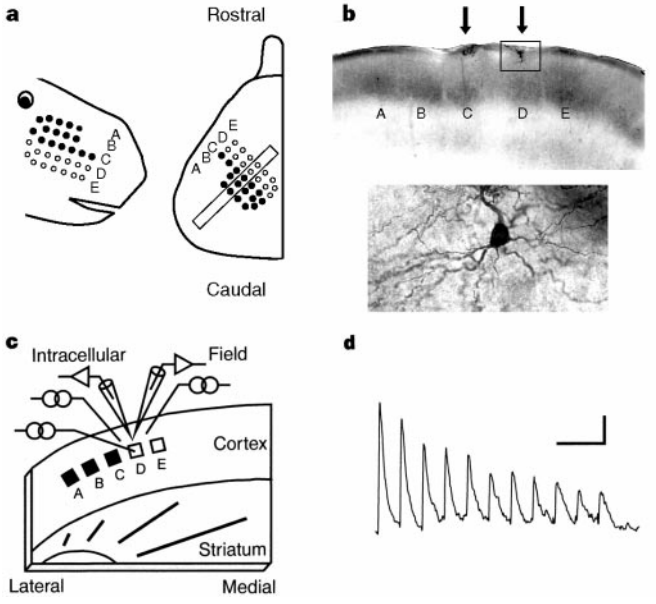

Figure 1 'Across whisker barrel row' brain slice preparation. **a**, Position of whiskers on the rat's snout and their map on the contralateral primary somatosensory cortex. Trimmed whiskers (here, D and E rows) are represented as empty circles. The schematic diagram of the left hemisphere shows the plane of section, 45° to the midline, for preparing brain slices. **b**, Combined bioctyin and cytochrome oxidase stain of a slice showing five whisker barrels. Arrows, cell bodies of filled pyramidal cells in layer 2 above C and D barrels. The box enclosing the neuron in the D barrel column is enlarged below. **c**, Arrangement of the recording and stimulating electrodes for the horizontal and vertical pathways on the slice. The barrels are coded as in **a**. The recording protocol is repeated in the same slice after the recording and stimulating electrodes are recentred above the C barrel column. **d**, Averaged response (three trials) evoked by stimulation at 10 Hz of the vertical layer 4–2 pathway in the C barrel column of the brain slice shown in **b**. Scale bars: 200 ms, 1 mV.

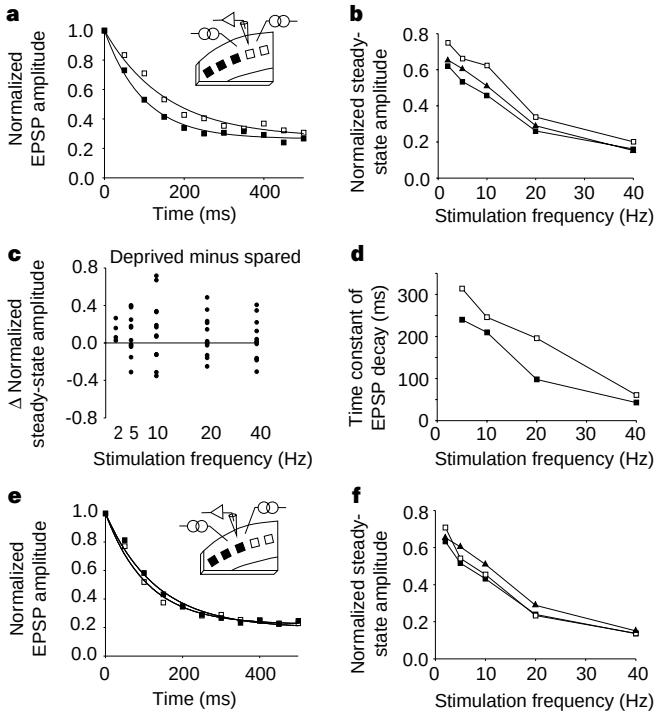

Figure 2 Short-term synaptic dynamics of horizontal pathways. **a**, Normalized EPSP amplitudes in deprived cortex evoked by 20 Hz stimulation of deprived (open squares, $n = 12$) and spared (filled squares, $n = 12$) cortex. Time constants of EPSP amplitude decay were derived from single exponential fits represented by the continuous lines. **b**, Normalized steady-state amplitude plotted against stimulation frequency for inputs to deprived cortex from deprived (open squares, $n = 12$) and spared (filled squares, $n = 12$) cortex compared with a control cortex (filled triangles, $n = 9$). **c**, Differences in normalized steady-state of deprived and spared inputs to deprived cortex from trimmed rats. **d**, Time constant of EPSP amplitude decay for deprived and spared inputs to deprived cortex plotted against frequency. **e**, Normalized EPSP amplitudes in spared cortex evoked by 20 Hz stimulation of deprived (open squares, $n = 12$) and spared (filled squares, $n = 12$) cortex. **f**, Normalized steady-state amplitude plotted against stimulation frequency for inputs to spared cortex from deprived (open squares, $n = 12$) and spared (filled squares, $n = 12$) cortex compared with control cortex (filled triangles, $n = 9$).

and 40 Hz (Fig 3b, c). The responses of control animals were similar to those in deprived cortex, but statistically different from those in spared cortex (mean difference, 0.06 ± 0.02, $P = 0.04$, paired t-test), indicating that sensory deprivation primarily induced changes in spared cortex. Increased depression in spared inputs compared with deprived inputs was accompanied by a shortening of the time constant of EPSP amplitude decay at 5 and 10 Hz, but not 20 and 40 Hz (Fig. 3d). In four cells (two spared, one deprived and one control) the stimulus train protocol in the layer 4–2 and layer 2–2 pathways was repeated with 200 μM 2-hydroxysaclofen, a GABA (γ-aminobutyric acid)$_B$ antagonist, in the artificial cerebrospinal fluid (ACSF). The normalized steady-state amplitude did not change significantly in either pathway, indicating that presynaptic $GABA_B$ receptors did not have an important role in stimulus-train-induced depression or the effects of sensory deprivation.

Our data indicated that sensory deprivation modified the synaptic dynamics of both horizontal and vertical pathways in supragranular cortex. Two questions arose. First, could the change in synaptic dynamics contribute to cortical map reorganization in supragranular cortex? Second, what caused the synaptic dynamics to change? To answer these questions we modified and extended a phenomenological model[17]. We refer to the EPSP amplitude during a stimulus train as the synaptic efficacy. The data we present have been normalized. In the model, normalized synaptic efficacy depends on stimulation frequency and two other parameters. S is the proportion of available synaptic resources used to generate an EPSP. This proportion can be thought of as the synaptic strength and, for simplicity, that is how we will refer to it. τ is the time constant with which synaptic resources recover after generating an EPSP. Note that we make a clear distinction between synaptic strength, which is a constant during the stimulus train, and synaptic efficacy, which varies. The model predicts that normalized EPSP amplitudes decay exponentially to a steady state during a stimulus train. Therefore, we used the normalized steady-state and time constant of EPSP amplitude decay extracted from our single exponential curve fits to calculate the values for synaptic strength and the recovery time constant at different stimulus frequencies.

We compared horizontal intracortical inputs from spared and deprived cortex onto layer 2 neurons in deprived cortex. The mean synaptic strengths of spared-to-deprived inputs were significantly greater than those of deprived-to-deprived inputs at all frequencies studied (input from spared cortex, 0.35 ± 0.03; deprived cortex, 0.21 ± 0.03; $P < 0.001$, paired t-test) (Fig. 4a), with synaptic strengths in control cortex having intermediate values (0.27 ± 0.04). The calculated recovery time constants for deprived, spared and control cortex were not different (input from spared cortex, 480 ± 40 ms; deprived cortex, 520 ± 70 ms; control cortex, 650 ± 100 ms; one-way analysis of variance, $P = 0.25$). We performed a similar analysis of the horizontal intracortical inputs onto layer 2 pyramidal cells in spared cortex. The mean synaptic strengths were similar (spared-to-spared, 0.33 ± 0.07; deprived-to-spared, 0.32 ± 0.05; $P = 0.67$, paired t-test) with both tending to be bigger than controls (inputs from spared cortex, $P = 0.06$; deprived cortex, $P = 0.05$) (Fig. 4a). The mean recovery time constants were not statistically different (spared cortex, 590 ± 130 ms; deprived cortex, 510 ± 60 ms; $P = 0.21$, paired t-test). We made an independent measurement of the recovery time constant by presenting test responses after the stimulus train. The mean recovery time constant was similar to that extracted from stimulus train data (mean $\tau = 660 \pm 110$ ms, $n = 5$).

In the vertical layer 4–2 pathway, there was a significant increase in synaptic strength in spared cortex, but not in deprived cortex, when compared to controls (spared, 0.34 ± 0.07 vs control, 0.28 ± 0.06 ($P = 0.01$, paired t-test); deprived, 0.29 ± 0.06). The differences in the normalized steady-state of vertical pathways in deprived and spared cortex showed frequency selectivity. Therefore, we compared the synaptic strengths of vertical pathways derived from single stimulation frequencies. We found a statistically significant difference in synaptic strength at 10 Hz (spared, 0.30 ± 0.04; deprived, 0.23 ± 0.02; $P = 0.03$, paired t-test). The mean recovery time constant did not change with sensory deprivation (spared, 1,020 ± 210 ms vs. deprived, 1,190 ± 180 ms; $P = 0.554$, paired t-test).

Our results indicate that an increase in synaptic strength accounts for the changes in synaptic dynamics that we found experimentally. We have no data on how synaptic strength changes over the trimming period. However, 2-deoxyglucose studies of trimmed rats indicate increased activity in spared cortex within hours of

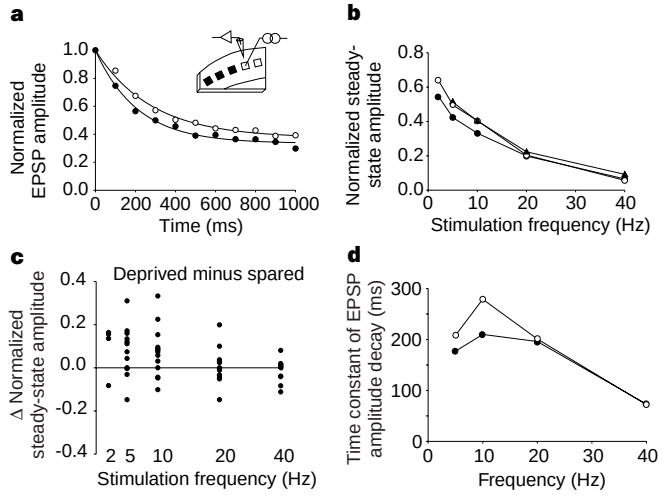

Figure 3 Short-term synaptic dynamics of vertical pathways. **a**, Normalized EPSP amplitudes evoked by 10 Hz stimulation in deprived (open circles, $n = 12$) and spared (filled circles, $n = 12$) cortex. **b**, Normalized steady-state amplitude plotted against frequency for deprived (open circles, $n = 13$), spared (filled circles, $n = 13$) and control (filled triangles, $n = 9$) inputs. **c**, Difference between normalized steady-states of deprived and spared cortex for each pair of cells from trimmed rats. **d**, Time constant of EPSP amplitude decay for layer 4–2 pathways in deprived and spared cortex.

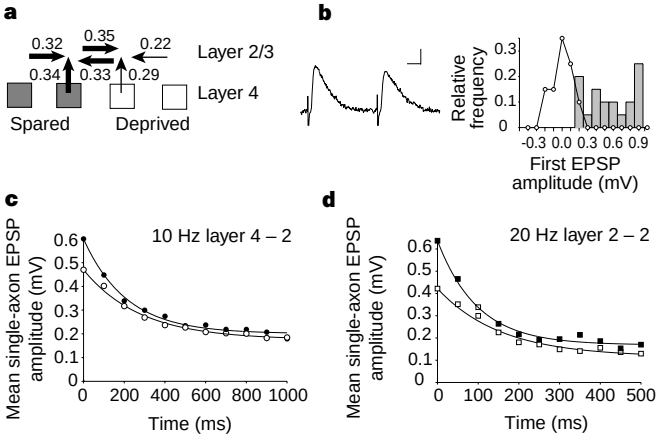

Figure 4 Sensory deprivation changes synaptic strength and synaptic efficacy. **a**, Synopsis of mean synaptic strengths over 5–40 Hz for vertical and horizontal pathways around the junction of spared and deprived cortex. Tail of the arrow, site of stimulation; tip, recording site. Width of arrows scaled with respect to control values for the horizontal (0.27) and vertical (0.28) pathways. **b**, Example of the mean response of 20 successive trails using minimal stimulation protocol on the layer 4–2 pathway. The amplitudes of the first EPSP (grey bars) and noise (open circles) are shown. Scale bars: 20 ms, 0.2 mV. **c**, Estimated synaptic efficacy for an average single-axon response to a 10-Hz stimulus train in the layer 4–2 pathways of deprived (open circles) and spared (filled circles). **d**, Estimated single-axon synaptic efficacy of the deprived-to-deprived (open circles) and spared-to-deprived (filled circles) horizontal pathways in response to a 20-Hz train.

trimming[18] and, in adults, single-unit recordings show increased firing of layer 4 cells by the third day post-trim[19]. Thus, we believe that an increase in synaptic strength is consistent with sensory deprivation strengthening that pathway rather than preventing it from becoming weaker as the rat ages. The opposite, sensory deprivation weakening inputs, probably applies to horizontal pathways in deprived cortex where there is a decrease in cell firing at points away from the junction between deprived and spared cortex[7]. The pattern of our results for the horizontal pathways onto deprived cortex and the vertical pathway in spared cortex (increased synaptic strength and unchanged recovery time constant) is the same as that reported for long-term potentiation (LTP) induced by pairing presynaptic firing with postsynaptic depolarization *in vitro*[15]. This raises the possibility that LTP may have caused the change in synaptic dynamics that we found. However, this remains to be determined. The horizontal pathway from spared to deprived cortex, which shows the greatest change in synaptic strength, is the pathway where pronounced anatomical changes are found after prolonged sensory deprivation[20,21]. This indicates that the same mechanisms that modify short-term synaptic dynamics may also drive the longer-term anatomical changes.

Understanding how a change in short-term synaptic dynamics could lead to functional reorganization of cortical maps requires a comparison of the synaptic efficacies of different pathways when the same number of axons have been stimulated. We reasoned that if we found the mean single-axon EPSP amplitude then we could use our stimulus train data to estimate the single-axon synaptic efficacy for each pathway. Therefore, after completing our stimulus train protocol in a pathway, we measured a single-axon evoked EPSP in the same pathway using a minimal stimulation paradigm. This was done for eight pairs of cells (five trimmed and three control slices) in both vertical and horizontal pathways. There are technical and interpretational problems associated with minimal stimulation. However, we were still able to draw some simple conclusions using these data.

Single-axon EPSPs varied greatly between cells, as expected[22] (Fig. 4b). However, there was a strong correlation between the computed synaptic strength of the pathways used for minimal stimulation and their measured mean single-axon EPSP amplitudes ($n = 8$, synaptic strengths at 20 Hz, $r = 0.94$, $P < 0.01$, Pearson product moment correlation). We used these data to estimate the synaptic efficacy of mean single-axon inputs onto layer 2/3 cells. The results showed that pathways with larger synaptic strengths were changed in two ways: the amplitude of the initial EPSP in the train was increased, and the EPSP amplitude depressed faster during the stimulus train (Fig. 4c, d). The net effect, comparing vertical layer 4–2 pathways, was that EPSPs in spared cortex were larger than those in deprived and control cortex throughout a 10 Hz stimulus train (Fig. 4c). When we compared horizontal deprived-to-deprived and spared-to-deprived pathways, we found that layer 2–2 EPSPs from spared cortex remained larger throughout a 20 Hz stimulus train (Fig. 4d). At higher frequencies, EPSP amplitudes cross over during the stimulus train, owing to the greater depression of the pathway with higher synaptic strength. However, steady-state EPSPs approach the same values as noted with paired recordings[15].

Our results show, for the first time, to our knowledge, that sensory experience modifies the short-term dynamics of excitatory synapses in the neocortex. Furthermore, our findings might help to explain how modifications of excitatory circuitry in supragranular cortex may contribute to expansion of cortical maps after sensory deprivation lasting days. Recordings in primary somatosensory cortex from freely moving rats using their whiskers reveal a 7–12 Hz oscillation synchronized with whisker protraction[23]. Typically, whisker deflection causes neurons in layer 4 to fire 0–2 spikes. Thus, sensory deprivation increases the synaptic efficacy of the layer 4–layer 2 pyramidal cell pathway in spared cortex during whisking and, therefore, the likelihood that spared layer 2 neurons will fire. The horizontal intracortical pathways amplify the changes in the vertical pathway inputs for two reasons. The synaptic efficacy of the horizontal pathway from spared cortex to deprived cortex is increased, and the synaptic efficacy of inputs to layer 2 neurons in deprived cortex from other pyramidal cells in deprived cortex is decreased. The result is that layer 2 neurons in deprived cortex receive a much larger proportion of their synaptic input from layer 2 neurons in spared cortex, compared with control conditions. Thus, firing of layer 2 neurons in spared and deprived cortex is more likely to be synchronized and the cortical representation of spared inputs expands. The corollary of our sensory deprivation protocol is a perceptual learning paradigm where practice on a task leads to improved discrimination. Cortical maps also reorganize during perceptual learning[2]. Mechanisms similar to those that we have described here may be involved. We suggest that our findings may exemplify a more general mechanism that regulates the allocation of cortical space in primary sensory cortex. □

Methods

Slice preparation. On the day of recording, rats had all whiskers trimmed acutely to blind the electrophysiologist to the rat's sensory history. Brain slices 400 μm thick were cut at 45° to the midline (Fig. 1), stored in an incubation chamber at 34 °C for 1 h and then checked for the presence of five whisker barrel rows[14]. Suitable slices were transferred to a submersion chamber at room temperature and bathed in ACSF flowing at 2 ml min^{-1} and containing (in mM): NaCl 124, KCl 3, NaH_2PO_4 1.25, $NaHCO_3$ 26, dextrose 10, $MgCl_2$ 1 and $CaCl_2$ 2, and saturated with 95%/5% O_2/CO_2. Ultrasmall bipolar stimulation electrodes (25 μm tip, FHC) were located in layer 4 and layer 2/3 (Fig. 1c). Field potentials in layer 2/3 were recorded with micropipettes (0.5–1 MΩ) filled with 2 mM bicuculline methiodide dissolved in ACSF. We recorded EPSPs from neurons in the immediate vicinity of the field potential electrode with sharp microelectrodes (70–100 MΩ) filled with 3 M potassium acetate and 1% biocytin. An EPSP of ~5 mV was evoked to prevent activation of voltage-gated dendritic channels that could modify EPSP amplitude[24]. We ensured that fast IPSPs were blocked by stimulating either layer 2 or layer 4 while depolarizing layer 2/3 neurons with current pulses and checking for the presence of a hyperpolarizing potential overlapping the EPSP[25]. NMDA (*N*-methyl-D-aspartate) receptors were blocked with 50 μM D,L-2-amino-5-phosphopentanoic acid (AP5, Sigma) in the ACSF. We estimated the recovery time constant for short interstimulus intervals by fitting a single exponential to test responses ≤500 ms from the end of the stimulus train. When recordings from the first barrel column were completed, we moved stimulating and recording electrodes to the other barrel column at the junction of deprived and spared cortex and repeated the recording protocol. The slice was fixed after recording was completed and the cell type and location of recorded neurons were confirmed histologically using a combined biocytin and cytochrome oxidase stain (Fig. 1b). Synaptic responses were digitized at 10 kHz. Data acquisition and signal analysis were done with Labview (National Instruments). Single exponential curve fitting was done using the Marquardt–Levenburg algorithm in SigmaPlot (SPSS).

Minimal stimulation. Current stimulus intensity was reduced to evoke a single-axon response[26–28]. Twenty trials of paired stimuli (100 ms interstimulus interval) given every 10 s were averaged to ensure that the mean first and second EPSPs had the same latency and time to peak. Measurements averaged over a 2 ms window were then made on successive traces of EPSP amplitude and baseline noise. We corrected for error in the mean amplitude due to baseline variability by subtracting the baseline mean from the amplitude mean. Single-axon EPSP amplitudes from each pathway were averaged to calculate the mean single-axon EPSP amplitude. The mean synaptic strength of the smaller number of pathways used for minimal stimulation was different on occasions from the mean synaptic strength calculated from pooled stimulus train data. To correct for this, we multiplied mean single-axon EPSPs by the ratio of the synaptic strength calculated from pooled stimulus train data for that pathway to the mean synaptic strength of the pathways used for minimal stimulation.

Model of synaptic depression. The model[17] proposes that a pathway possesses a fixed amount of synaptic resources that exist in one of three states: recovered, active and inactive. An EPSP is modelled by the transfer of a constant proportion of synaptic resources S from the recovered pool into

the active pool. These resources then relax into the recovered pool through the inactive pool. We assume that the decay from active to inactive pools is rapid so that the effective time constant for relaxation into the recovered pool is τ. For simplicity, we express the total amount of synaptic resources as the maximal EPSP amplitude A, which is the magnitude of the evoked EPSP when all the synaptic resources are used. EPSP amplitudes during a stimulus train are given by the product of the synaptic strength and the synaptic resources in the recovered pool at the time of the action potential. Combining the model with the experimental observations that there is a linear relationship between the dendritic excitatory postsynaptic current (EPSC) and somatic EPSP when the somatic EPSP is less than ~5 mV[24], and that somatic EPSPs add linearly[29], we derived an equation relating normalized EPSP amplitudes during a stimulus train. After k stimulus intervals of a regular stimulus train of frequency f, normalized $\mathrm{EPSP}_k = \{S \cdot e^{-(1/\tau - f \cdot \ln(1-S))t} + (e^{1/(f\tau)} - 1)\}/(e^{1/(f\tau)} - (1 - S))$. Thus, a continuous curve drawn through normalized EPSP amplitudes evoked by the stimulus train has an exponential form with a steady state of $(e^{1/(f\tau)} - 1)/(e^{1/(f\tau)} - (1 - S))$ and a time constant of decay of $(1/\tau - f \cdot \ln(1 - S))^{-1}$.

Received 22 March; accepted 3 June 1999.

1. Buonomano, D. V. & Merzenich, M. M. Cortical plasticity: from synapses to maps. *Annu. Rev. Neurosci.* **21,** 149–186 (1998).
2. Gilbert, C. D. Adult cortical dynamics. *Physiol. Rev.* **78,** 467–485 (1998).
3. Merzenich, M. M. *et al.* Progression of changes following median nerve section in the cortical representation of the hand in areas 3b and 1 in adult owl and squirrel monkeys. *Neuroscience* **10,** 639–665 (1983).
4. Robertson, D. & Irvine, D. Plasticity of frequency organization in auditory cortex of guinea pigs with partial unilateral deafness. *J. Comp. Neurol.* **282,** 456–471 (1989).
5. Kaas, J. H. *et al.* Reorganization of retinotopic cortical maps in adult mammals after lesions of the retina. *Science* **248,** 229–231 (1990).
6. Glazewski, S. & Fox, K. Time course of experience-dependent synaptic potentiation and depression in barrel cortex of adolescent rats. *J. Neurophysiol.* **75,** 1714–1729 (1996).
7. Gilbert, C. D. & Wiesel, T. N. Receptive field dynamics in adult primary visual cortex. *Nature* **356,** 150–152 (1992).
8. Fox, K. A critical period for experience-dependent synaptic plasticity in rat barrel cortex. *J. Neurosci.* **12,** 1826–1838 (1992).
9. Diamond, M. E., Huang, W. & Ebner, F. F. Laminar comparison of somatosensory cortical plasticity. *Science* **265,** 1885–1888 (1994).
10. Kirkwood, A., Rioult, M. C. & Bear, M. F. Experience-dependent modification of synaptic plasticity in visual cortex. *Nature* **381,** 526–528 (1996).
11. Glazewski, S., Chen, C.-M., Silva, A. & Fox, K. Requirement for α-CaMKII in experience-dependent plasticity of the barrel cortex. *Science* **272,** 421–423 (1996).
12. Garraghty, P. E. & Muja, N. NMDA receptors and plasticity in adult primate somatosensory cortex. *J. Comp. Neurol.* **367,** 319–326 (1996).
13. Carvell, G. E. & Simons, D. J. Biometric analyses of vibrissal tactile discrimination in the rat. *J. Neurosci.* **10,** 2638–2648 (1990).
14. Welker, C. & Woolsey, T. A. Structure of layer IV in the somatosensory neocortex of the rat: description and comparison with the mouse. *J. Comp. Neurol.* **158,** 437–454 (1974).
15. Markram, H. & Tsodyks, M. Redistribution of synaptic efficacy between neocortical pyramidal cells. *Nature* **382,** 807–810 (1996).
16. Abbot, L. F., Varela, J. A., Sen, K. & Nelson, S. B. Synaptic depression and cortical gain control. *Science* **275,** 220–224 (1997).
17. Tsodyks, M. V. & Markram, H. The neural code between neocortical pyramidal neurons depends on neurotransmitter release probability. *Proc. Natl Acad. Sci. USA* **94,** 719–723 (1997).
18. McCasland, J. S. & Woolsey, T. A. High-resolution 2-deoxyglucose mapping of functional cortical columns in mouse barrel cortex. *J. Comp. Neurol.* **278,** 555–569 (1988).
19. Armstrong-James, M. Diamond, M. E. & Ebner, F. F. An innocuous bias in whisker use in adult rats modifies receptive fields of barrel cortex neurons. *J. Neurosci.* **14,** 6978–6991 (1994).
20. Darian-Smith, C. & Gilbert, C. D. Axonal sprouting accompanies functional reorganization in adult cat striate cortex. *Nature* **368,** 737–740 (1994).
21. Florence, S. L., Taub, H. B. & Kaas, J. H. Large-scale sprouting of cortical connections after peripheral injury in adult macaque monkeys. *Science* **282,** 1117–1121 (1998).
22. Mason, A., Nicoll, A. & Stratford, K. Synaptic transmission between individual pyramidal neurons of the rat visual cortex in vitro. *J. Neurosci.* **11,** 72–84 (1991).
23. Nicolelis, M. A. L., Baccala, L. A., Lin, R. C. S. & Chapin, J. K. Sensorimotor encoding by synchronous neural ensemble activity at multiple levels of the somatosensory system. *Science* **268,** 1353–1358 (1995).
24. Stuart, G. & Sakmann, B. Amplification of EPSPs by axosomatic sodium channels in neocortical pyramidal neurons. *Neuron* **15,** 1065–1076 (1995).
25. Connors, B. W., Malenka, R. C. & Silva, L. R. Two inhibitory postsynaptic potentials, and $GABA_A$ receptor-mediated responses in neocortex of rat and cat. *J. Physiol. (Lond.)* **406,** 443–468 (1988).
26. Dobrunz, L. E. & Stevens, C. F. Heterogeneity of release probability, facilitation, and depletion at central synapses. *Neuron* **18,** 995–1008 (1997).
27. Raastad, M., Storm, J. F. & Andersen, P. Putative single quantum and single fibre excitatory postsynaptic currents show similar amplitude range and variability in rat hippocampal slices. *Eur. J. Neurosci.* **4,** 113–117 (1992).
28. Volgushev, M., Voronin, L. L., Chistiakova, M., Artola, A. & Singer, W. All-or-none excitatory postsynaptic potentials in the rat visual cortex. *Eur. J. Neurosci.* **7,** 1751–1760 (1995).
29. Cash, S. & Yuste, R. Input summation by cultured pyramidal neurons is linear and position-independent. *J. Neurosci.* **18,** 10–15 (1998).

Acknowledgements. This work was supported by a Wellcome Trust Advanced Training Fellowship to G.T.F. and a grant to B.W.C. from NIH. We thank S. Patrick for technical assistance with histology; A. Akima for discussions on the optimal slicing angle; D. Pinto for checking the mathematics; and M. Bear, J. Gibson, M. Beierlein and D. Pinto for helpful comments on a earlier version of the manuscript. G.T.F. thanks R. Jones and D. Smith for encouragement with the current project.

Correspondence and requests for materials should be addressed to B.W.C. (e-mail: Barry_Connors@brown.edu).

Selective inhibition of cocaine-seeking behaviour by a partial dopamine D_3 receptor agonist

Maria Pilla*†, Sylvie Perachon*‡§, François Sautel‡, Fabrice Garrido‖, André Mann‖, Camille G. Wermuth‖, Jean-Charles Schwartz‡, Barry J. Everitt† & Pierre Sokoloff‡

† *Department of Experimental Psychology, University of Cambridge, Downing Street, Cambridge CB2 3EB, UK*
‡ *Unité de Neurobiologie et Pharmacologie Moléculaire, INSERM U 109, Centre Paul Broca, 2ter rue d'Alésia, 75014 Paris, France*
§ *Laboratoire Bioprojet, 9 rue Rameau, 75002 Paris, France*
‖ *Laboratoire de Pharmacochimie de la Communication Cellulaire CNRS ERS 655, Faculté de Pharmacie, 74 route du Rhin BP 24, 67401 Illkirsch, France*
* *These authors contributed equally to this work.*

Environmental stimuli that are reliably associated with the effects of many abused drugs, especially stimulants such as cocaine, can produce craving and relapse in abstinent human substance abusers[1–4]. In animals, such cues can induce and maintain drug-seeking behaviour and also reinstate drug-seeking after extinction[5–7]. Reducing the motivational effects of drug-related cues might therefore be useful in the treatment of addiction[3]. Converging pharmacological[8,9], human post-mortem[10] and genetic[11] studies implicate the dopamine D_3 receptor[12] in drug addiction. Here we have designed BP 897, the first D_3-receptor-selective agonist, as assessed *in vitro* with recombinant receptors and *in vivo* with mice bearing disrupted D_3-receptor genes. BP 897 is a partial agonist *in vitro* and acts *in vivo* as either an agonist or an antagonist. We show that BP 897 inhibits cocaine-seeking behaviour that depends upon the presentation of drug-associated cues, without having any intrinsic, primary rewarding effects. Our data indicate that compounds like BP 897 could be used for reducing the drug craving and vulnerability to relapse that are elicited by drug-associated environmental stimuli.

Until now, it has proved difficult to identify or design a D_3

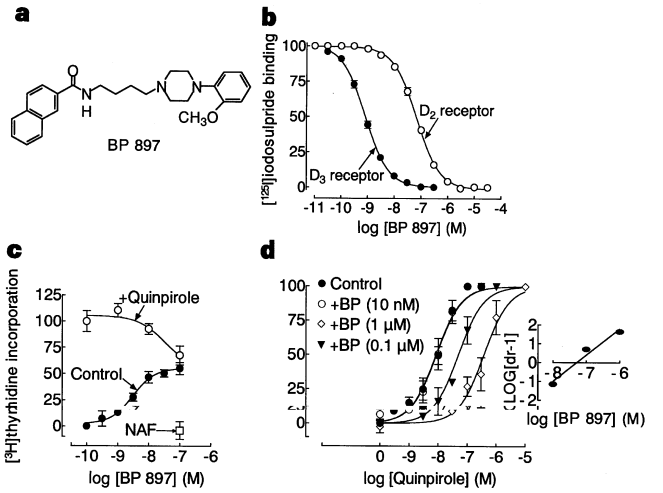

Figure 1 BP 897 is a potent and partial D_3 receptor agonist and a weak D_2 receptor antagonist. **a**, Chemical structure of BP 897. **b**, Inhibition by BP 897 of [^{125}I]iodosulpride binding to recombinant D_2 and D_3 receptors. **c**, In NG 108-15 cells expressing the D_3 receptor, BP 897 activated mitogenesis and this response was antagonized by the preferential D_3 receptor antagonist nafadotride (NAF, 1 μM). BP 897 also partially antagonized the response induced by quinpirole (10 nM). **d**, In CHO cells expressing the D_2 receptor, BP 897, while having no effect by itself, reversibly antagonized quinpirole-induced mitogenesis. The Schild plot (inset) allowed us to calculate a pK_i value for BP 897 of 7.29 (K_i = 51 nM).